ACS APPLIED MATERIALS & INTERFACES

Research Article

Cite This: ACS Appl. Mater. Interfaces 2018, 10, 5618−5625

www.acsami.org

Microporous Luminescent Metal−Organic Framework for a Sensitive and Selective Fluorescence Sensing of Toxic Mycotoxin in Moldy Sugarcane

Dan Tian,[†,§] Xiao-Jing Liu,[†] Rui Feng,[†] Jia-Li Xu,[†] Jian Xu,[*,†] Rong-Ying Chen,[†] Ling Huang,[§] and Xian-He Bu[*,†,‡]

[†]School of Materials Science and Engineering, National Institute for Advanced Materials, TKL of Metal- and Molecule-Based Material Chemistry, Collaborative Innovation Center of Chemical Science and Engineering (Tianjin), Nankai University, Tianjin 300350, P. R. China

[‡]State Key Laboratory of Elemento-Organic Chemistry, College of Chemistry, Nankai University, Tianjin 300071, P. R. China

[§]Key Laboratory of Flexible Electronics (KLOFE) & Institute of Advanced Materials (IAM), National Jiangsu Synergistic Innovation Center for Advanced Materials (SICAM), Nanjing Tech University (NanjingTech), 30 South Puzhu Road, Nanjing 211816, P. R. China

Supporting Information

ABSTRACT: Food contamination by toxic mycotoxins not only causes a considerable loss in economy, but importantly poses a huge threat to human health through accidental ingestion. Hence, it is an ongoing and imperative need to develop a convenient, cost-effective method for the detection of the mycotoxin-infected agricultural commodities. To this end, we herein fabricated a novel metal−organic framework-derived composite material that displays a strong solid-state emission in the visible region, by attaching a frequently used fluorescent label, fluorescein isothiocyanate (FITC), via guest adsorption. Significantly, owing to the inherent pH-responsive conformational changes of FITC, the resulting composite material provides, to the best of our knowledge, the first example of the sensitive and selective fluorescence sensing toward 3-nitropropionic acid, which, as a major naturally occurring mycotoxin in moldy sugarcane, has been closely linked to poisoning episodes in human beings and animals.

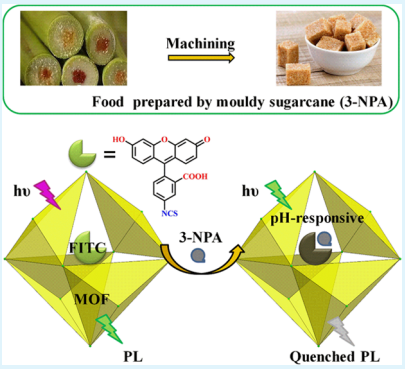

KEYWORDS: *metal−organic framework, luminescence sensing, mycotoxin detection, fluorescein isothiocyanate, 3-nitropropionic acid*

1. INTRODUCTION

Food spoilage is a global issue, especially more serious in developing countries. Ingesting food contaminated by mycotoxins (i.e., toxic secondary metabolites produced by organisms of the fungus kingdom,[1,2] popularly known as molds) poses a poisoning risk to human beings and animals. Each year, at least 2% of the food products are contaminated by molds worldwide, causing a great economic loss. Among various toxic mycotoxins, 3-nitropropionic acid (3-NPA) is the secondary metabolite of Arthrinium fungus from moldy sugarcane and has already been identified as an etiologic agent of intoxications.[3,4] As a naturally occurring plant mycotoxin, this toxic substance has been closely linked to poisoning episodes in human beings and animals,[5,6] potentially causing Huntington disease symptoms, central nervous system dysfunction, and brain damage in children. Because it is difficult to differentiate the food items at the onset of spoilage or in the early stage of being spoiled, accidental ingestion of moldy sugarcane, that is, a fatal food poisoning by 3-NPA, is still popular in 13 of all 34 provinces in China.

More seriously, sugarcane is also one major raw source of sucrose, which plays a central role as an additive in food production and consumption all over the world. In 2013 alone, about 175 million metric tons of sucrose sugars were produced worldwide for human consumption. Unfortunately, the chemical stability of mycotoxin 3-NPA could promise its survival through modern industrial sugar refinement and subsequent food manufacture processes. Thus, monitoring the content of toxic 3-NPA and preventing its entrance into the food chain of human consumption via moldy sugarcane are vitally crucial for human society. At present, the currently prevailing methods for mycotoxin detection include thin layer chromatography, high performance liquid chromatography, gas chromatography, and so forth.[7−9] However, these external monitoring technologies usually require expensive instruments and show less efficiency in real-time detection applications because of poor portability, intensive laboring, high cost, and

Received: October 17, 2017
Accepted: January 19, 2018
Published: January 19, 2018

DOI: 10.1021/acsami.7b15764
ACS Appl. Mater. Interfaces 2018, 10, 5618−5625

complicated operation. Therefore, the development of a simple, rapid, and low-cost approach for the detection of highly toxic mycotoxins, for example, 3-NPA, is extremely urgent for global food security.

Owing to the excellent convenience and quick response, fluorescence sensing has developed as a promising detection technique, especially for the small molecules of biomedical, food, and environmental interests.[10−13] Of the widely used organic fluorophores, fluorescein isothiocyanate (FITC), a visible yellow-green-emitting dye molecule with strong emission and great photostability, has been widely used as a label to attach to various principal materials via a fluorescent-labeling technique for sensing applications.[14,15] Notably, the FITC dye molecules are pH-sensitive and can intrinsically exhibit the pH-dependent ratiometric fluorescence changes,[16,17] making them a superior sensor to acid analytes and thus potentially available to the detection of 3-NPA. However, a well-known issue largely impedes the sensing applications of FITC, that is, the fluorescence self-quenching phenomenon frequently encountered in their aggregated forms,[18] that is, the so-called aggregation-caused quenching (ACQ) effect. In this regard, some of the reported FITC-based composites, such as FITC-capped gold nanoparticles and FITC-capped carbon dots,[19−23] display stronger fluorescence intensity relative to pure FITC dyes, but are hampered by synthesis difficulty and poor recyclability.

Metal−organic frameworks (MOFs) composed of metal ions (or clusters) and organic ligands are a class of inorganic−organic hybrid crystalline materials[24−26] and exhibit immense potentials in a wide range of applications, such as gas storage,[27−29] sensing,[30−34] catalysis,[35−37] and so forth. Significantly, many beneficial features, including facile synthesis, tunable porosity, designable structures, and easy-to-functionalize surfaces, make MOFs suitable hosts for accommodating guest molecules and even endowing them with some specific functions. With these advantages, porous MOFs significantly offer a unique platform to incorporate organic fluorophores (e.g., FITC) to produce the solid-state luminescent materials with target-sensing properties. As examples, many such fluorescent MOFs have been fabricated and explored as sensors for the detection of small molecules,[38,39] implemented by monitoring the change in fluorescence readout and showing remarkable advantages such as high sensitivity, quick response, good reversibility, ready operability, and ease of visualization. In this regard, there have been three major strategies proposed for the engineering of MOF-based luminescent sensors: (i) anchoring the luminescent sensor molecules onto the reactive group of MOFs' organic ligands via postsynthetic modifications (Scheme 1a);[40,41] (ii) building MOF scaffolds starting from the organic building blocks decorated with luminescent sensor molecules (Scheme 1b); and[42−44] (iii) encapsulating the luminescent sensor molecules within MOFs' pores directly (Scheme 1c). Straightforwardly, the third making use of permanent porosity of MOFs is undoubtedly the simplest and most convenient one among the three and will not be influenced by the compatibility or interference between the introduced fluorophores and the formation of the desired MOF structures, and thereby has been extensively studied.

On the basis of the foregoing, we herein fabricated a novel microporous MOF, formulated as $[Cd(L)\cdot solvent]_n$ (**1**), and used it as a host to encapsulate the FITC dye molecules, for the effective sensing of 3-NPA, by which several severe issues can be addressed readily. First, the conjugation between FITC and the bridging ligands of **1** can largely prevent the transudation of these dye molecules highly sensitive to acidic analytes, ensuring the recyclability of the resulting sensor material. Second, the highly ordered and confined porous structure of **1** enables the effective isolation of FITC dye molecules within the framework, even in the case of high loadings, thus enhancing the output fluorescence signal by preventing the notorious ACQ effect. Third, the open channels of **1** allow a rapid and free diffusion of the analytes with proper sizes, which greatly facilitates the sensing operation throughout the process and is thus conducive to the responsivity and sensitivity of the sensor material.[45,46] As a result, the reported dye-functionalized MOF demonstrates, to the best of our knowledge, the first example of the selective and sensitive fluorescence-based detection of 3-NPA, reaching a high-level detection limit of 0.135 M.

Scheme 1. (a) Luminescent Sensor Molecules Are Anchored onto the Reactive Groups of MOFs' Organic Ligands via Postsynthetic Modifications; (b) Organic Building Blocks Decorated with Sensor Molecules Are Used to Build MOF Scaffolds; (c) Luminescent Sensor Molecules Are Encapsulated within MOFs' Pores Directly

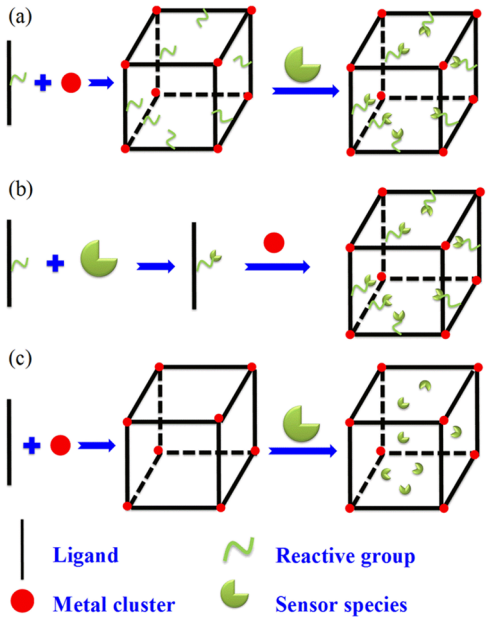

2. EXPERIMENTAL SECTION

2.1. Materials and General Methods. All of the chemicals used for synthesis are of analytical grade and commercially available. The IR spectra were measured on a Tensor 27 OPUS (Bruker) Fourier transform infrared (FT-IR) spectrometer with KBr pellets. Powder X-ray diffraction (PXRD) spectra were recorded on a Rigaku D/Max-2500 diffractometer at 40 kV, 100 mA for a Cu-target tube and a graphite monochromator. Thermogravimetric analyses (TGAs) were carried out on a Rigaku standard TG-DTA analyzer under N_2 with a heating rate of 10 °C min^{-1}, with an empty Al_2O_3 crucible used as the reference. Simulation of the PXRD pattern was carried out by single-crystal data and diffraction-crystal module of the mercury (Hg) program version 1.4.2, available free of charge via the Internet at http://www.iucr.org.

2.2. Synthesis of 1. A mixture of $Cd(NO_3)_2\cdot 6H_2O$ (0.07 mmol) and H_2L (0.035 mmol) in 6 mL of 3:3 (v/v) mixture of dimethylformamide (DMF)/C_2H_5OH was sealed in a 10 ml vial and heated at 85 °C for 72 h. The colorless crystals were collected by filtration, washed with DMF, and dried in air (yield: 15% based on H_2L). FT-IR (KBr pellets, cm^{-1}): 3284 (w), 3118 (w), 1679 (w), 1625

DOI: 10.1021/acsami.7b15764
ACS Appl. Mater. Interfaces 2018, 10, 5618−5625

(w), 1511 (s), 1388 (w), 1081 (w), 898 (s), 767 (s), 678 (s), 617 (s), 511 (w). Anal. Calcd for $CdC_{17}H_{12}N_5O_6$: C, 41.27; H, 2.44; N, 14.16%. Found: C, 41.96; H, 2.66; N, 14.13%.

2.3. X-ray Crystallography. Single-crystal X-ray diffraction measurement was carried out on Rigaku Saturn 70 diffractometer at 133(2) K for **1** with Mo Kα radiation (λ = 0.71073 Å). The structure was solved by direct methods using the SHELXS program of the SHELXTL package and refined with SHELXL.[47] All nonhydrogen atoms were refined with anisotropic temperature parameters. All atoms of ligands (except for O9 and O10) were split into two positions with occupancies of 0.5:0.5. SIMU was used to restrict the disordered atoms. It should be noted that some solvent molecules in the crystal are highly disordered and could not be modeled properly, so the diffused electron densities resulting from them were removed by the SQUEEZE routine in PLATON,[48] and the results were appended in the CIF files (CCDC: 1569436).

3. RESULTS AND DISCUSSION

3.1. Crystal Structure of 1. X-ray crystal structural analysis reveals that complex **1** exhibits a three-dimensional (3D) noninterpenetrated structure that crystallizes in the tetragonal space group *Pnna*. As shown in Figure S1a, the asymmetric unit of **1** consists of only two crystallographically independent Cd(II) ions: Cd(II)1 ion is coordinated by four carboxylate oxygen atoms from two L^{2-} ligands as well as two nitrogen atoms from another two L^{2-} ligands, whereas Cd(II)2 ion is surrounded by four carboxylate oxygen atoms from two L^{2-} ligands and two nitrogen atoms from another two L^{2-} ligands, as well as one carbonyl oxygen atom from one L^{2-} ligand, displaying a distorted pentagonal bipyramid geometry. In this structure, two Cd(II)1 and two Cd(II)2 ions link to each other via four −N−C−N− bridges to form a quadrinuclear {Cd_4} cluster (Figure 1a), with the distance of Cd1···Cd2 being 5.627 Å. Interestingly, each quadrinuclear {Cd_4} cluster gathers four pairs of two adjacent parallel L^{2-} ligands (the distance between them measuring 5.6 Å) in four different directions (Figure 1b). Note that, each L^{2-} ligand adopting a nearly planar geometry binds two Cd(II)1 and two Cd(II)2 ions to its coordination sites, that is, O/N atoms (Figure S1b).

On the basis of the connection modes, four {Cd_4} clusters arranged in an analogous tetrahedral mode are bridged together by five pairs of two parallel L^{2-} ligands (Figure 1c). For clarity, we denote the quadrinuclear {Cd_4} cluster in this tetrahedral unit as node P: the distances of P1···P2 and P1···P4 are 21.847 and 13.493 Å, respectively, and the P4 node lies 4.498 Å away from the plane involving the other three equivalent P nodes. Additionally, four analogous tetrahedral units are connected together by six vertex-sharing {Cd_4} clusters, consequently forming an octahedral cage with the internal diameter of 15 Å (Figure 1d). Therein, four of the eight faces are occupied by the tetrahedral units, whereas the other four still remain "open". In this octahedral chamber, the distance between the diagonal nodes (P) is 30.896 Å. Furthermore, the octahedral cages are packed together by {Cd_4} clusters to yield a 3D double-walled framework (Figures 1e and S2). With the four open faces of these octahedral cages, the resulting whole framework exhibits one-dimensional (1D) channels along the *a* direction (Figure 1e) with dimensions of ca. 9 × 14 $Å^2$ (without considering *van der Waals* radii), which are occupied by dimethylamine cations. The solvent accessible volume of **1** is estimated to be 62.8% per unit cell by PLATON[48] analysis. From the viewpoint of topology, each {Cd_4} cluster can be simplified as a tetragonally 4-connected node (Figure S3a), whereas the two pairs of half L^{2-} ligands in parallel arrangement can be viewed as linkers

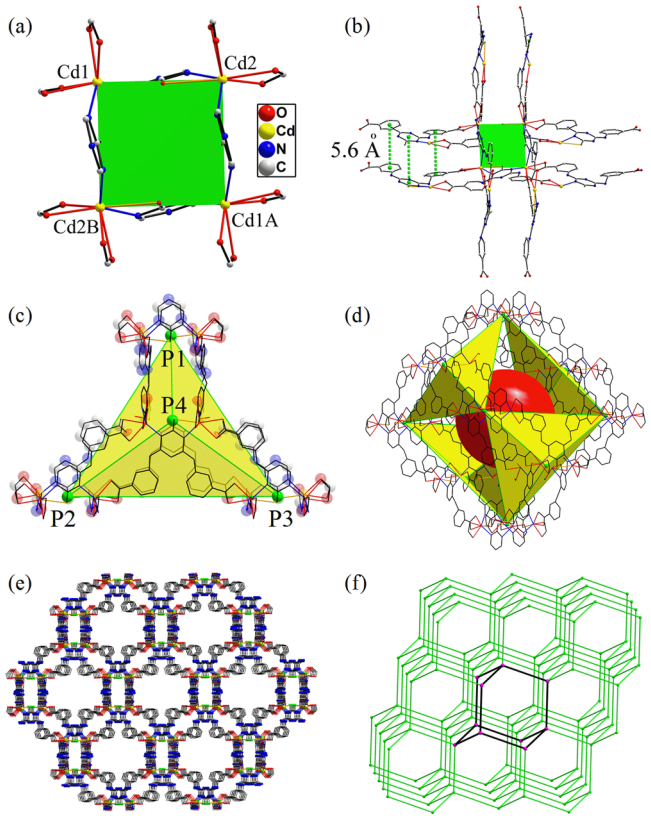

Figure 1. Structure of **1**: (a) Coordination environment of the Cd(II) ions (symmetry codes: $A = -1/2 + x, y, 2 - z$ and $B = 1/2 + x, y, 2 - z$). (b) Eight ligands connected by one Cd_4 cluster. (c) One face of the octahedral cage. (d) Presentation of the octahedral cages. (e) 3D framework viewed along the *a* axis. (f) Schematic illustration of the dia topology of the 3D network.

(Figure S3b). Thus, an infinite 4-connected net with dia topology and the long Schläfli symbol[49] of $6_2{\cdot}6_2{\cdot}6_2{\cdot}6_2{\cdot}6_2{\cdot}6_2$ are produced by TOPOS,[50,51] as illustrated in Figures 1f and S4.

3.2. Thermal and Chemical Stability of 1. Next, we conducted the examinations on the thermal stability of **1**, as well as its chemical stability in acidic, basic, and neutral aqueous solutions, as these are crucial for the industrial applications of a MOF material. The TGA result reveals that the framework of **1** was thermally stable up to 350 °C (Figure S5). As for the chemical stability of **1**, PXRD patterns were implemented to validate the crystallinity after being immersed in pure water for 3 d, whereas in hydrochloric acid (pH = 2−6) and sodium hydroxide (pH = 8−12) aqueous solutions for 24 h (Figure S6). Therein, all of the PXRD profiles of the treated samples are in good agreement with that of the as-prepared **1**. Nevertheless, the PXRD patterns after immersing the sample in aqueous solutions (pH = 3 and 10) for 48 h are not in complete agreement with the simulated pattern (Figure S7), implying a partial structural collapse. This discovery indicates that the framework of **1** possesses relatively good chemical stability in water and acidic or basic conditions that satisfy a basic requirement for quick optical sensing in a short time.

3.3. Encapsulation of FITC Molecules. The permanent porosity and remarkable stability performances of complex **1** provide the prerequisites for the encapsulation of the target FITC dye molecules of matching size and also the further functionalization for sensing purpose in practical environments. Conveniently, the integration of FITC dye molecules into the

DOI: 10.1021/acsami.7b15764
ACS Appl. Mater. Interfaces 2018, 10, 5618−5625

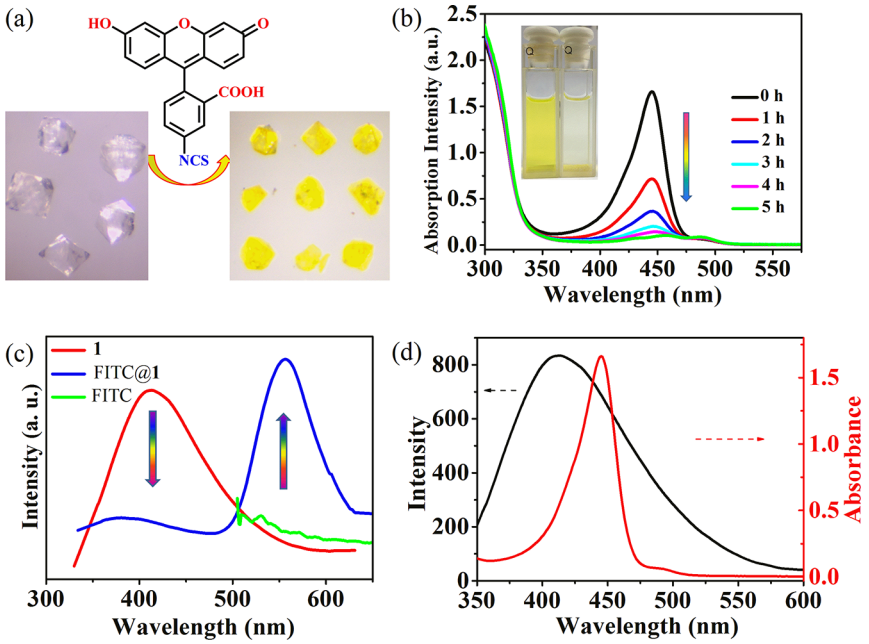

Figure 2. (a) Color change of complex **1** after being immersed in ethanol solution of FITC. (b) UV−vis spectra of the ethanol solutions of FITC with the freshly prepared **1**. Inset: Photographs of the color change of the ethanol solution upon dye adsorption. (c) Solid-state emission spectra of **1** and FITC@**1** (λ_{ex} = 340 nm), FITC (λ_{ex} = 490 nm). (d) Absorption spectrum (red) of FITC dyes in the liquid state and emission spectrum of **1** (black) in the solid state.

MOF is rather straightforward, which can be readily accomplished by soaking the sample of **1** into the ethanol solution of FITC. As Figure 2a illustrates, along with this loading process, the crystals of **1** with octahedral morphology display an appreciable color change from colorless (**1**) to yellow (FITC@**1**). Further, the confocal images of FITC@**1** reveal a uniform distribution of FITC molecules in the framework after encapsulation, which is also an evidence that the target FITC dyes truly diffused into the open channels without a prominent aggregation occurred (Figure S8). Importantly, while the concentration of FITC in ethanol dramatically decreased with the passage of loading time, revealed by UV−vis spectra (Figure 2b), the crystalline integrity of **1** was not degraded as confirmed by the PXRD profiles (Figure S9).

The adsorbent capability of **1** for FITC from ethanol could be quantitatively evaluated by monitoring the variation in the absorption spectra of the FITC ethanol solution. Herein, we calculated the adsorption capacity (q) of the adsorbent by employing the equation of $(C_0 - C_t)V/m$, in which V (L) is the volume of FITC solution, m (g) is the mass of complex **1**, whereas C_0 and C_t (mg/L) refer to the initial and residual concentrations of FITC solution, respectively. According to the data from Figure 2b, the adsorption of FITC by complex **1** reached saturation after 5 h, with the saturated uptake (q_e) being approximately 29 mg/g. It should be mentioned that **1** also has the ability to adsorb other common dye molecules with appropriate sizes under similar conditions, including rhodamine 6G, methyl orange, and methylene blue (Figure S10).

3.4. Pore Characterization by N_2 Adsorption. The permanent porosity is one of the most important attributes of MOFs, as it plays a pivotal role in many practical applications. Thus, we conducted the N_2 adsorption experiments on both of the samples of **1** and FITC@**1** at 77 K (Figure 3). Before adsorption, complex **1** was completely activated by immersing the sample in ethanol for 96 h, and the ethanol solvent was changed every 12 h. Consequently, the Brunauer−Emmett−

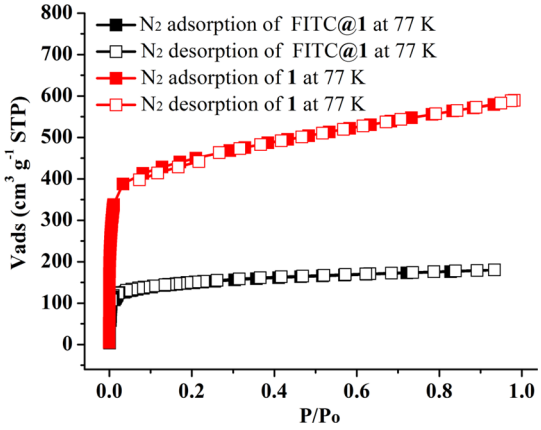

Figure 3. N_2 sorption isotherm for **1** and FITC@**1** at 77 K.

Teller (BET) was estimated to be 1504 $m^2\ g^{-1}$ for the activated **1** and 559 $m^2\ g^{-1}$ for FITC@**1**, respectively. The relatively smaller BET of FITC@**1**, to some extent, indicates a successful encapsulation of FITC dye molecules. The fitting of the adsorption data according to the Horvath−Kawazoe method demonstrates that the pore size distribution of **1** ranges from 0.5 to 1.5 nm (Figure S11), indicating the microporous nature of the framework.

3.5. Luminescence Behaviors and Sensing Properties. After successful encapsulation of FITC labels, we then made a comprehensive study and comparison of the photoluminescence properties of **1**, FITC, and FITC@**1** at room temperature (Figure 2c). Upon excitation at 490 nm, the pure FITC powder had almost no emissions, whereas FITC@**1** displayed a very strong FITC-based emission band centered at 560 nm (green). Obviously, such an apparent enhancement in emission intensity should be attributed to the confinement effect of **1**'s framework. Specifically, once the FITC dye molecules were entrapped in the pores, their intramolecular

DOI: 10.1021/acsami.7b15764
ACS Appl. Mater. Interfaces 2018, 10, 5618−5625

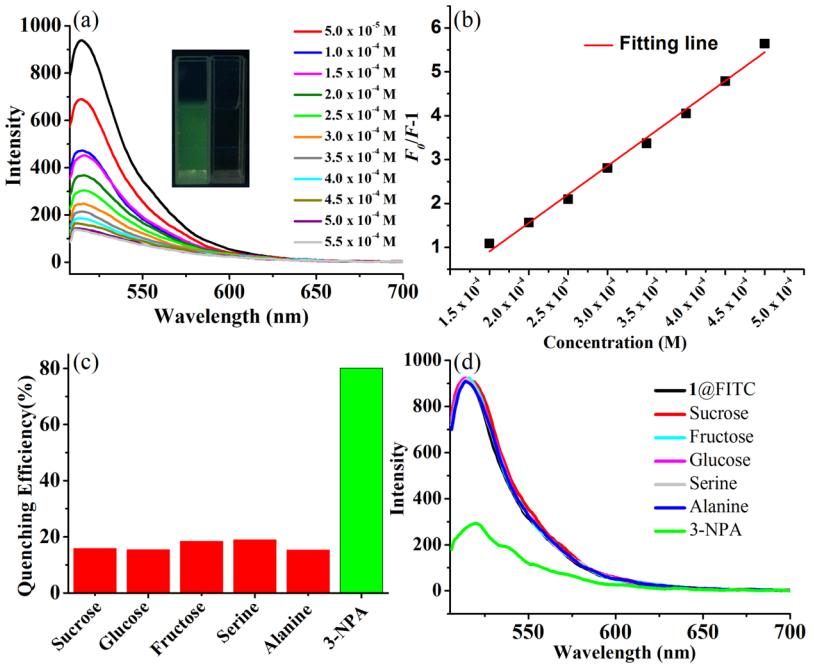

Figure 4. (a) Emission spectra (λ_{ex} = 490 nm) of FITC@**1** dispersed in water with the addition of different contents of 3-NPA. (b) Linear relationship between quenching efficiency and 3-NPA content fitted by the Stern−Volmer (SV) equation. (c) Quenching efficiency of FITC@**1** dispersed in water with the addition of different analytes. The emission intensities were selected at their maxima. (d) Emission spectra (λ_{ex} = 490 nm) of FITC@**1** dispersed in water after addition of five interfering substances (60 μL) and a subsequent addition of 3-NPA (60 μL).

torsional motion would be largely limited, which helps in diminishing the ACQ effect by reducing the $\pi-\pi$ interactions between the aromatic rings of the framework and those of FITC molecules. On the other hand, under a 320 nm UV irradiation, complex **1** emitted a blue light with the maximum wavelength at 415 nm. Further analysis revealed that an accessible energy transfer from the MOF to the dye molecules was likely to cause such an apparent emission shift between **1** and FITC@**1**. As shown in Figure 2d, there is a considerable spectral overlap between the absorption band of FITC and the emission band of **1**, promising an efficient fluorescence resonance energy transfer (FRET) from the framework to FITC.[52,53] Further, with the dye concentration increasing, the fluorescence intensity of the green emission band (FITC@**1**) displayed an incremental enhancement, whereas that of the blue emission (**1**) was gradually quenched, which is strongly in support of the proposed FRET energy-transfer mechanism.

Evidently, the strong emission intensity of the obtained composite material and the intrinsic pH responsivity of FITC thus pave the way for the feasible fluorescence detection of acidic small molecules in real life scenarios. Bearing this in mind, we then explored the responsivity and sensitivity of FITC@**1** to the presence of an acidic mycotoxin, naturally occurring in moldy sugarcane, that is, 3-NPA, by monitoring the emission signal change of FITC@**1** suspension before and after the addition of the analyte. As shown in Figure 4a, the emission intensity of FITC@**1** began to decrease upon the addition of 5×10^{-5} M 3-NPA and was remarkably quenched at the concentration of 5.5×10^{-4} M with a quenching efficiency of 85.6%. Notably, in this experiment, the detection limit estimated in terms of $3\sigma/k$ (k: slope, σ: standard) reached about 0.135 M (Figure S12), indicating high sensitivity of this FITC-functionalized MOF toward 3-NPA. The photoluminescence quenching constant can be quantitatively evaluated by the SV equation: $(F_0/F) = 1 + K_{sv}[Q]$,[54,55] in which K_{sv} is the quenching constant, [Q] is the molar concentration of 3-NPA analyte, F_0 and F are the photoluminescence intensities before and after the addition of 3-NPA analyte, respectively. As shown in Figure 4b, the SV plot is linearly correlated with the 3-NPA content (R^2 = 0.9989) at low concentrations and gives the highest K_{sv} value of 1.29×10^4 M^{-1}. On the other hand, the recyclability of this sensor material was also examined because of its importance to practical applications. When 6×10^{-4} M 3-NPA was added into the suspension of FITC@**1** (10 mg of crystal and 10 mL of H_2O), its luminescence intensity at 520 nm decreased by 91.8% and can be recovered to 83.4% by simply washing with weak alkaline solution three times. The regenerated sample was then reused in the following consecutive detection−activation runs, and the quenching efficiency reduced to 39% after three cycles (Figure S13). All these facts suggest FITC@**1** to be an ideal sensor for a trace amount of 3-NPA on account of its high quenching constant, linear scaling, low detection concentration, and recyclability.

Except for 3-NPA, several other common constituents of sugarcane, including sucrose, glucose, fructose, serine, and alanine, were also considered to imitate the practical detection of spoiled sugarcane. Therein, the finely ground sample of FITC@**1** (3 mg) was initially immersed in aqueous solution (3 mL) and subsequently treated by ultrasonication for 30 min and aged for 3 d to form a stable emulsion. Then, the fluorescence responses of the composite were recorded when separately titrating equal amounts of different disruptors listed above. The emission spectra shown in Figure 4c illustrate that the emission intensity of the suspension of FITC@**1** was quenched to ca. 80% when the content of 3-NPA approached 4×10^{-4} M, whereas, with the addition of the same amount of sucrose, glucose, fructose, serine, or alanine, the maximum change in emission intensity was less than 20%. Obviously, these results indicate that the composite FITC@**1** can effectively differentiate several major nontoxic constituents of

DOI: 10.1021/acsami.7b15764
ACS Appl. Mater. Interfaces 2018, 10, 5618−5625

sugarcane from the toxic 3-NPA by displaying a highly selective fluorescence quenching response. For a comprehensive assessment of the sensing ability of a material, its antiinterference ability should also be examined. Thus, we sequentially introduced the five interfering substances (i.e., sucrose, glucose, fructose, serine, and alanine) into the current system. As shown in Figure 4d, the fluorescence intensity of the suspension was almost unchanged with the addition of five substances (3×10^{-5} M), but was acutely decreased after the addition of 3-NPA (3×10^{-5} M). These results then suggest that this material has an outstanding antiinterference ability and is thereby feasible for the detection of moldy sugarcane.

It is well-established that FITC is an important pH-responsive fluorescence probe and has various tautomeric forms (e.g., lactone, carboxylate anion, and carboxylic acid).[56] These fluorescein derivatives are defined in terms of the form of the carboxyl group at the 2-position of the benzene moiety. According to the literature, FITC appears predominantly in its neutral form, as the intramolecular spirolactone preferentially forms below pH = 7.0.[56] Easily, the FITC molecule containing the lactone ring has a relatively weak conjugation and thereby exhibits a weak emission even in the isolated form in solution. In comparison, its ring-open form could largely promote the fluorescence intensity because of the presence of the intramolecular moiety with stronger conjugation. Therefore, it is likely that the FITC dye molecules encapsulated in **1**'s framework underwent a conformational change from the ring-open form to the intramolecular spirolactone form, induced by the acid analysts that diffused within the open channels and were in close proximity to FITC (Figure 5a,b). In addition, this

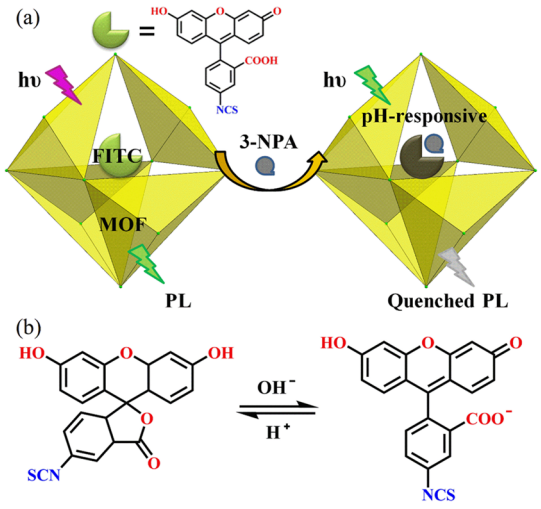

Figure 5. (a) Schematic illustration of the underlying mechanism of the selective sensing of FITC@**1** toward 3-NPA. (b) pH-dependent conversion between two isomers in FITC molecule with quinoid and lactone structures.

conformational conversion accounts for the fluorescence quenching selectivity of FITC@**1** to the acidic molecule (3-NPA) among the tested analytes (sucrose, glucose, fructose, serine, and alanine). To testify this, we then examined the pH values of acidic analytes with different concentrations. The results indicate that the pH values of 10^{-3}, 10^{-4}, 10^{-5}, and 10^{-6} M 3-NPA are about 3.02, 3.67, 4.52, and 5.16, respectively, in good agreement with the degrees of fluorescence quenching observed experimentally and thus in support of our analysis.

4. CONCLUSIONS

In summary, a microporous Cd(II)-based luminescent MOF was successfully constructed with aromatic ligand H_2L and d^{10} configuration metal ion Cd(II) under solvothermal conditions. This porous material can adsorb a certain amount of dye molecules of appropriate sizes, especially including FITC, one of the most common fluorescence labels. Immobilizing the FITC dye molecules into this MOF via guest adsorption could not only improve the FITC-originated emission intensity by taking advantage of the confinement effect of the framework, but also could preserve their intrinsic pH responsivity to acidic small molecules. It is because the open channels of **1** allow the diffusion of the analytes and thus their close proximity to FITC dyes. As a result, the obtained composite material displayed a highly sensitive and selective fluorescence quenching response to toxic 3-NPA, which is an acidic mycotoxin, and significantly may cause adverse health effects on human beings via consumption of moldy sugarcane. Specifically, in response to the analyte-induced pH variations, the FITC molecules in **1** would undergo a conformational conversion from the ring-open form to the intramolecular spirolactone form, resulting in a considerable change in conjugation that accounts for the observed fluorescence-quenching phenomenon. The significance of this work is to provide not only a low-cost, easily portable, and readily available fluorescence sensor for the detection of toxic 3-NPA mycotoxin, but also a new insight into the development and engineering of the functionalized MOF materials.

■ ASSOCIATED CONTENT

Supporting Information

The Supporting Information is available free of charge on the ACS Publications website at DOI: 10.1021/acsami.7b15764.

Additional figures, TGA profiles, PXRD patterns, UV–vis spectra, and emission spectra (PDF)

Crystallographic data of **1** (CIF)

■ AUTHOR INFORMATION

Corresponding Authors

*E-mail: jxu@nankai.edu.cn (J.X.).

*E-mail: buxh@nankai.edu.cn (X.-H.B.).

ORCID

Jian Xu: 0000-0001-9347-1095

Ling Huang: 0000-0003-1244-3522

Xian-He Bu: 0000-0002-2646-7974

Notes

The authors declare no competing financial interest.

■ ACKNOWLEDGMENTS

D.T. and X.-J.L. contributed equally to this work. We thank Dr. Yu-Hui Luo (Huaihai Institute of Technology) for the crystallographic refinement. This work was financially supported by the NNSF of China (21771113, 21601086, 21290171, and 21421001), and the Natural Science Foundation of Jiangsu Province (BK20160994).

■ REFERENCES

(1) Matumba, L.; Van Poucke, C.; Ediage, E. N.; Saeger, S. D. Keeping mycotoxins away from the food: Does the existence of regulations have any impact in Africa? *Crit. Rev. Food Sci. Nutr.* **2017**, *57*, 1584–1592.

DOI: 10.1021/acsami.7b15764
ACS Appl. Mater. Interfaces 2018, 10, 5618–5625

(2) Rubert, J.; Righetti, L.; Stranska-Zachariasova, M.; Dzuman, Z.; Chrpova, J.; Dall'Asta, C.; Hajslova, J. Untargeted metabolomics based on ultra-high-performance liquid chromatography−high-resolution mass spectrometry merged with chemometrics: A new predictable tool for an early detection of mycotoxins. *Food Chem.* **2017**, *224*, 423−431.
(3) Ming, L. Moldy Sugarcane Poisoning−A Case Report with a Brief Review. *J. Toxicol. Clin. Toxicol.* **1995**, *33*, 363−367.
(4) Sulyok, M.; Krska, R.; Schuhmacher, R. Application of an LC−MS/MS based multi-mycotoxin method for the semi-quantitative determination of mycotoxins occurring in different types of food infected by moulds. *Food Chem.* **2010**, *119*, 408−416.
(5) Malik, J.; Karan, M.; Dogra, R. Ameliorating effect of Celastrus paniculatus standardized extract and its fractions on 3-nitropropionic acid induced neuronal damage in rats: possible antioxidant mechanism. *Pharm. Biol.* **2017**, *55*, 980−990.
(6) Wang, L.; Wang, J.; Yang, L.; Zhou, S.-M.; Guan, S.-Y.; Yang, L.-K.; Shi, Q.-X.; Zhao, M.-G.; Yang, Q. Effect of Praeruptorin C on 3-nitropropionic acid induced Huntington's disease-like symptoms in mice. *Biomed. Pharmacother.* **2017**, *86*, 81−87.
(7) Hollmann, M.; Razzazi-Fazeli, E.; Grajewski, J.; Twaruzek, M.; Sulyok, M.; Böhm, J. Detection of 3-nitropropionic acid and cytotoxicity inMucor circinelloides. *Mycotoxin Res.* **2008**, *24*, 140−150.
(8) Majak, W.; McDiarmid, R. E. Detection and quantitative determination of 3-nitropropionic acid in bovine urine. *Toxicol. Lett.* **1990**, *50*, 213−220.
(9) Muir, A. D.; Majak, W. Quantitative determination of 3-nitropropionic acid and 3-nitropropanol in plasma by HPLC. *Toxicol. Lett.* **1984**, *20*, 133−136.
(10) Wu, Y.; Wei, P.; Pengpumkiat, S.; Schumacher, E. A.; Remcho, V. T. Development of a Carbon Dot (C-Dot)-Linked Immunosorbent Assay for the Detection of Human α-Fetoprotein. *Anal. Chem.* **2015**, *87*, 8510−8516.
(11) Tian, D.; Li, Y.; Chen, R.-Y.; Chang, Z.; Wang, G.-Y.; Bu, X.-H. A luminescent metal−organic framework demonstrating ideal detection ability for nitroaromatic explosives. *J. Mater. Chem. A* **2014**, *2*, 1465−1470.
(12) Wang, B.; Lv, X.-L.; Feng, D.; Xie, L.-H.; Zhang, J.; Li, M.; Xie, Y.; Li, J.-R.; Zhou, H.-C. Highly Stable Zr(IV)-Based Metal−Organic Frameworks for the Detection and Removal of Antibiotics and Organic Explosives in Water. *J. Am. Chem. Soc.* **2016**, *138*, 6204−6216.
(13) Pramanik, S.; Zheng, C.; Zhang, X.; Emge, T. J.; Li, J. New Microporous Metal−Organic Framework Demonstrating Unique Selectivity for Detection of High Explosives and Aromatic Compounds. *J. Am. Chem. Soc.* **2011**, *133*, 4153−4155.
(14) Song, C.; Liu, J.; Li, J.; Liu, Q. Dual FITC lateral flow immunoassay for sensitive detection of Escherichia coli O157:H7 in food samples. *Biosens. Bioelectron.* **2016**, *85*, 734−739.
(15) Sun, S.; Ning, X.; Zhang, G.; Wang, Y.-C.; Peng, C.; Zheng, J. Dimerization of Organic Dyes on Luminescent Gold Nanoparticles for Ratiometric pH Sensing. *Angew. Chem., Int. Ed.* **2016**, *55*, 2421−2424.
(16) He, C.; Lu, K.; Lin, W. Nanoscale Metal−Organic Frameworks for Real-Time Intracellular pH Sensing in Live Cells. *J. Am. Chem. Soc.* **2014**, *136*, 12253−12256.
(17) Ke, C.-Y.; Wu, Y.-T.; Tseng, W.-L. Fluorescein-5-isothiocyanate-conjugated protein-directed synthesis of gold nanoclusters for fluorescent ratiometric sensing of an enzyme−substrate system. *Biosens. Bioelectron.* **2015**, *69*, 46−53.
(18) Ren, C.; Wang, H.; Mao, D.; Zhang, X.; Fengzhao, Q.; Shi, Y.; Ding, D.; Kong, D.; Wang, L.; Yang, Z. When Molecular Probes Meet Self-Assembly: An Enhanced Quenching Effect. *Angew. Chem., Int. Ed.* **2015**, *54*, 4823−4827.
(19) Liu, J.; Liu, J.; Liu, W.; Zhang, H.; Yang, Z.; Wang, B.; Chen, F.; Chen, H. Triple-Emitting Dumbbell Fluorescent Nanoprobe for Multicolor Detection and Imaging Applications. *Inorg. Chem.* **2015**, *54*, 7725−7734.
(20) Lin, C.-Y.; Liu, C.-H.; Tseng, W.-L. Fluorescein isothiocyanate-capped gold nanoparticles for fluorescent detection of reactive oxygen species based on thiol oxidation and their application for sensing glucose in serum. *Anal. Methods* **2010**, *2*, 1810−1815.
(21) Hu, B.; Zhao, Y.; Zhu, H.-Z.; Yu, S.-H. Selective Chromogenic Detection of Thiol-Containing Biomolecules Using Carbonaceous Nanospheres Loaded with Silver Nanoparticles as Carrier. *ACS Nano* **2011**, *5*, 3166−3171.
(22) Zhu, X.; Jin, H.; Gao, C.; Gui, R.; Wang, Z. Ratiometric, visual, dual-signal fluorescent sensing and imaging of pH/copper ions in real samples based on carbon dots-fluorescein isothiocyanate composites. *Talanta* **2017**, *162*, 65−71.
(23) Du, F.; Ming, Y.; Zeng, F.; Yu, C.; Wu, S. A low cytotoxic and ratiometric fluorescent nanosensor based on carbon-dots for intracellular pH sensing and mapping. *Nanotechnology* **2013**, *24*, 365101.
(24) Tian, D.; Chen, Q.; Li, Y.; Zhang, Y.-H.; Chang, Z.; Bu, X.-H. A Mixed Molecular Building Block Strategy for the Design of Nested Polyhedron Metal−Organic Frameworks. *Angew. Chem., Int. Ed.* **2014**, *53*, 837−841.
(25) Huang, R.-W.; Wei, Y.-S.; Dong, X.-Y.; Wu, X.-H.; Du, C.-X.; Zang, S.-Q.; Mak, T. C. W. Hypersensitive dual-function luminescence switching of a silver-chalcogenolate cluster-based metal−organic framework. *Nat. Chem.* **2017**, *9*, 689−697.
(26) Nugent, P.; Belmabkhout, Y.; Burd, S. D.; Cairns, A. J.; Luebke, R.; Forrest, K.; Pham, T.; Ma, S. Q.; Space, B.; Wojtas, L.; Eddaoudi, M.; Zaworotko, M. J. Porous materials with optimal adsorption thermodynamics and kinetics for CO_2 separation. *Nature* **2013**, *495*, 80−84.
(27) Van de Voorde, B.; Bueken, B.; Denayer, J.; De Vos, D. Adsorptive separation on metal−organic frameworks in the liquid phase. *Chem. Soc. Rev.* **2014**, *43*, 5766−5788.
(28) Zhai, Q.-G.; Bu, X.; Zhao, X.; Li, D.-S.; Feng, P. Pore Space Partition in Metal−Organic Frameworks. *Acc. Chem. Res.* **2017**, *50*, 407−417.
(29) Lin, Y.; Kong, C.; Zhang, Q.; Chen, L. Metal-Organic Frameworks for Carbon Dioxide Capture and Methane Storage. *Adv. Energy Mater.* **2017**, *7*, 1601296.
(30) Xu, H.; Fang, M.; Cao, C.-S.; Qiao, W.-Z.; Zhao, B. Unique (3,4,10)-Connected Lanthanide−Organic Framework as a Recyclable Chemical Sensor for Detecting Al^{3+}. *Inorg. Chem.* **2016**, *55*, 4790−4794.
(31) Zhou, J.; Li, H.; Zhang, H.; Li, H.; Shi, W.; Cheng, P. A Bimetallic Lanthanide Metal−Organic Material as a Self-Calibrating Color-Gradient Luminescent Sensor. *Adv. Mater.* **2015**, *27*, 7072−7077.
(32) Li, Y.; Zhang, S.; Song, D. A Luminescent Metal−Organic Framework as a Turn-On Sensor for DMF Vapor. *Angew. Chem., Int. Ed.* **2013**, *52*, 710−713.
(33) Peng, J.; Teoh, C. L.; Zeng, X.; Samanta, A.; Wang, L.; Xu, W.; Su, D.; Yuan, L.; Liu, X.; Chang, Y.-T. Development of a Highly Selective, Sensitive, and Fast Response Upconversion Luminescent Platform for Hydrogen Sulfide Detection. *Adv. Funct. Mater.* **2016**, *26*, 191−199.
(34) Song, X.-Z.; Song, S.-Y.; Zhao, S.-N.; Hao, Z.-M.; Zhu, M.; Meng, X.; Wu, L.-L.; Zhang, H.-J. Single-Crystal-to-Single-Crystal Transformation of a Europium(III) Metal−Organic Framework Producing a Multi-responsive Luminescent Sensor. *Adv. Funct. Mater.* **2014**, *24*, 4034−4041.
(35) An, B.; Zhang, J.; Cheng, K.; Ji, P.; Wang, C.; Lin, W. Confinement of Ultrasmall Cu/ZnOx Nanoparticles in Metal−Organic Frameworks for Selective Methanol Synthesis from Catalytic Hydrogenation of CO_2. *J. Am. Chem. Soc.* **2017**, *139*, 3834−3840.
(36) Kaneti, Y. V.; Tang, J.; Salunkhe, R. R.; Jiang, X.; Yu, A.; Wu, K. C.-W.; Yamauchi, Y. Nanoarchitectured Design of Porous Materials and Nanocomposites from Metal-Organic Frameworks. *Adv. Mater.* **2017**, *29*, 1604898.
(37) Wu, C.-D.; Zhao, M. Incorporation of Molecular Catalysts in Metal−Organic Frameworks for Highly Efficient Heterogeneous Catalysis. *Adv. Mater.* **2017**, *29*, 1605446.
(38) Hu, Z.; Lustig, W. P.; Zhang, J.; Zheng, C.; Wang, H.; Teat, S. J.; Gong, Q.; Rudd, N. D.; Li, J. Effective Detection of Mycotoxins by a

DOI: 10.1021/acsami.7b15764
ACS Appl. Mater. Interfaces 2018, 10, 5618−5625

Highly Luminescent Metal−Organic Framework. *J. Am. Chem. Soc.* **2015**, *137*, 16209−16215.
(39) Hao, J.-N.; Yan, B. Determination of Urinary 1-Hydroxypyrene for Biomonitoring of Human Exposure to Polycyclic Aromatic Hydrocarbons Carcinogens by a Lanthanide-functionalized Metal-Organic Framework Sensor. *Adv. Funct. Mater.* **2017**, *27*, 1603856.
(40) Gao, W.-Y.; Wu, H.; Leng, K.; Sun, Y.; Ma, S. Inserting CO_2 into Aryl C-H Bonds of Metal−Organic Frameworks: CO_2 Utilization for Direct Heterogeneous C-H Activation. *Angew. Chem., Int. Ed.* **2016**, *55*, 5472−5476.
(41) Zhang, L.; Jian, Y.; Wang, J.; He, C.; Li, X.; Liu, T.; Duan, C. Post-modification of a MOF through a fluorescent-labeling technology for the selective sensing and adsorption of Ag^+ in aqueous solution. *Dalton Trans.* **2012**, *41*, 10153−10155.
(42) Li, H.; Feng, X.; Guo, Y.; Chen, D.; Li, R.; Ren, X.; Jiang, X.; Dong, Y.; Wang, B. A malonitrile-functionalized metal-organic framework for hydrogen sulfide detection and selective amino acid molecular recognition. *Sci. Rep.* **2014**, *4*, 4366.
(43) Cho, W.; Lee, H. J.; Choi, G.; Choi, S.; Oh, M. Dual Changes in Conformation and Optical Properties of Fluorophores within a Metal−Organic Framework during Framework Construction and Associated Sensing Event. *J. Am. Chem. Soc.* **2014**, *136*, 12201−12204.
(44) He, J.; Yee, K.-K.; Xu, Z.; Zeller, M.; Hunter, A. D.; Chui, S. S.-Y.; Che, C.-M. Thioether Side Chains Improve the Stability, Fluorescence, and Metal Uptake of a Metal−Organic Framework. *Chem. Mater.* **2011**, *23*, 2940−2947.
(45) Rowsell, J. L. C.; Yaghi, O. M. Strategies for Hydrogen Storage in Metal−Organic Frameworks. *Angew. Chem., Int. Ed.* **2005**, *44*, 4670−4679.
(46) Yang, Q.; Zhong, C. Molecular Simulation of Adsorption and Diffusion of Hydrogen in Metal−Organic Frameworks. *J. Phys. Chem. B* **2005**, *109*, 11862−11864.
(47) Sheldrick, G. M. *SHELXTL NT*, version 5.1 (Program for Solution and Refinement of Crystal Structures); University of Göttingen: Göttingen, Germany, 1997.
(48) Spek, A. L. Single-crystal structure validation with the program PLATON. *J. Appl. Crystallogr.* **2003**, *36*, 7−13.
(49) O'Keeffe, M.; Hyde, S. T. Vertex symbols for zeolite nets. *Zeolites* **1997**, *19*, 370−374.
(50) Blatov, V. A.; Shevchenko, A. P.; Serezhkin, V. N. J. TOPOS3.2: a new version of the program package for multipurpose crystal-chemical analysis. *J. Appl. Crystallogr.* **2000**, *33*, 1193.
(51) Blatov, V. A.; Shevchenko, A. P.; Proserpio, D. M. Applied Topological Analysis of Crystal Structures with the Program Package ToposPro. *Cryst. Growth Des.* **2014**, *14*, 3576−3586.
(52) Chen, L.; Honsho, Y.; Seki, S.; Jiang, D. Light-Harvesting Conjugated Microporous Polymers: Rapid and Highly Efficient Flow of Light Energy with a Porous Polyphenylene Framework as Antenna. *J. Am. Chem. Soc.* **2010**, *132*, 6742−6748.
(53) Yu, J.; Cui, Y.; Xu, H.; Yang, Y.; Wang, Z.; Chen, B.; Qian, G. Confinement of pyridinium hemicyanine dye within an anionic metal-organic framework for two-photon-pumped lasing. *Nat. Commun.* **2013**, *4*, 2719.
(54) Lukat, G. S.; Stock, A. M.; Stock, J. B. Divalent Metal Ion Binding to the CheY Protein and Its Significance to Phosphotransfer in Bacterial Chemotaxis. *Biochemistry* **1990**, *29*, 5436−5442.
(55) Shi, Z.-Q.; Guo, Z.-J.; Zheng, H.-G. Two luminescent Zn(II) metal−organic frameworks for exceptionally selective detection of picric acidexplosives. *Chem. Commun.* **2015**, *51*, 8300−8303.
(56) Hirabayashi, K.; Hanaoka, K.; Takayanagi, T.; Toki, Y.; Egawa, T.; Kamiya, M.; Komatsu, T.; Ueno, T.; Terai, T.; Yoshida, K.; Uchiyama, M.; Nagano, T.; Urano, Y. Analysis of Chemical Equilibrium of Silicon-Substituted Fluorescein and Its Application to Develop a Scaffold for Red Fluorescent Probes. *Anal. Chem.* **2015**, *87*, 9061−9069.

DOI: 10.1021/acsami.7b15764
ACS Appl. Mater. Interfaces 2018, 10, 5618−5625